AD-A136 561 CALCULATION OF CUMULATIVE DISTRIBUTIONS AND DETECTION PROBABILITIES IN CO..(U) CALIFORNIA UNIV SAN DIEGO LA JOLLA DEPT OF ELECTRICAL ENGINEE.. C W HELSTROM 1/1

UNCLASSIFIED 17 OCT 83 AFOSR-TR-83-1237 AFOSR-82-0343 F/G 12/1 NL

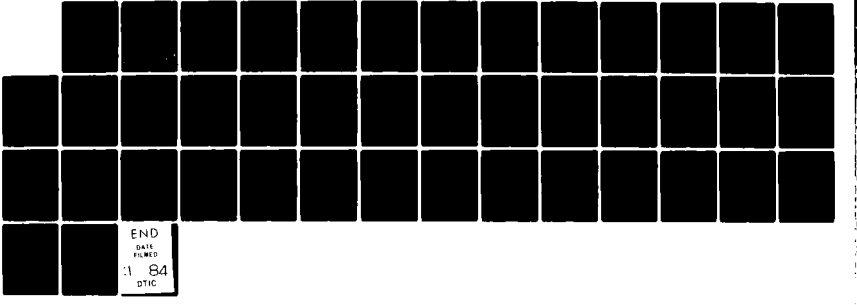

END

DATE FILMED

1 84

DTIC

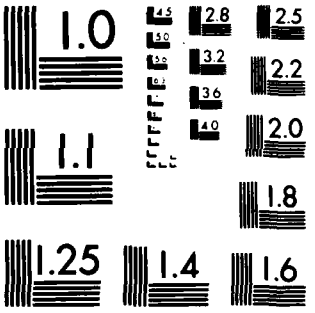

UNCLASSIFIED

SECURITY CLASSIFICATION OF THIS PAGE

(4)

REPORT DOCUMENTATION PAGE

1a. REPORT SECURITY CLASSIFICATION: UNCLASSIFIED	1b. RESTRICTIVE MARKINGS
2a. SECURITY CLASSIFICATION AUTHORITY	3. DISTRIBUTION/AVAILABILITY OF REPORT: Approved for public release; distribution unlimited.
2b. DECLASSIFICATION/DOWNGRADING SCHEDULE	
4. PERFORMING ORGANIZATION REPORT NUMBER(S)	5. MONITORING ORGANIZATION REPORT NUMBER(S): AFOSR-TR- 83-1237
6a. NAME OF PERFORMING ORGANIZATION: University of California (San Diego)	6b. OFFICE SYMBOL (If applicable):
6c. ADDRESS (City, State and ZIP Code): Electrical Engineering & Computer Science Department, C-014, La Jolla CA 92037	7a. NAME OF MONITORING ORGANIZATION: Air Force Office of Scientific Research
8a. NAME OF FUNDING/SPONSORING ORGANIZATION: AFOSR	8b. OFFICE SYMBOL (If applicable): NM
8c. ADDRESS (City, State and ZIP Code): Bolling AFB DC 20332	7b. ADDRESS (City, State and ZIP Code): Directorate of Mathematical & Information Sciences, Bolling AFB DC 20332
	9. PROCUREMENT INSTRUMENT IDENTIFICATION NUMBER: AFOSR-82-0343
	10. SOURCE OF FUNDING NOS.

PROGRAM ELEMENT NO.	PROJECT NO.	TASK NO.	WORK UNIT NO.
61102F	2304	A5	

11. TITLE (Include Security Classification): SEE REMARKS (on back)

12. PERSONAL AUTHOR(S): Carl W. Helstrom

13a. TYPE OF REPORT	13b. TIME COVERED	14. DATE OF REPORT (Yr., Mo., Day)	15. PAGE COUNT
Interim	FROM 1/10/82 TO 30/9/83	17 OCT 83	40

16. SUPPLEMENTARY NOTATION

17. COSATI CODES		
FIELD	GROUP	SUB. GR

18. SUBJECT TERMS (Continue on reverse if necessary and identify by block number): Numerical integration; detection; photomultipliers; probability distribution.

19. ABSTRACT (Continue on reverse if necessary and identify by block number)

Methods were investigated for evaluating cumulative distributions of continuous random variables of known moment-generating function by numerical quadrature of a contour integral in the complex plane whose integrand involves that function. Applications so far treated were to the detection of radar signals, both fading and unfading, in receivers with constant threshold or with a variable threshold determined by a measurement of the ambient noise (constant-false-alarm-rate receivers), and to the distribution of the average power of a Gaussian random process. Similar methods were studied for finding the cumulative distributions of positive-integral valued random variables by a numerical contour integration involving their probability generating functions, with application to evaluating the distribution of the number of electrons at the output of a photomultiplier.

20. DISTRIBUTION/AVAILABILITY OF ABSTRACT	21. ABSTRACT SECURITY CLASSIFICATION
UNCLASSIFIED/UNLIMITED ☒ SAME AS RPT. ☐ DTIC USERS ☐	UNCLASSIFIED

22a. NAME OF RESPONSIBLE INDIVIDUAL	22b. TELEPHONE NUMBER (Include Area Code)	22c. OFFICE SYMBOL
Dr. Robert T. Smythe	(202) 767-5028	NM

DD FORM 1473, 83 APR EDITION OF 1 JAN 73 IS OBSOLETE. UNCLASSIFIED

SECURITY CLASSIFICATION OF THIS PAGE

84 01 04 125

AD-A136561

DTIC FILE COPY

DTIC ELECTE JAN 04 1984 S E

ITEM #11, TITLE: CALCULATION CUMULATIVE DISTRIBUTIONS AND DETECTIVE PROBABILITIES IN COMMUNICATION AND OPTICS

Annual Report, 1982-83
Grant AFOSR-82-0343

Calculation of Cumulative Distributions and Detection Probabilities in Communications and Optics

Carl W. Helstrom

Department of Electrical Engineering & Computer Sciences
University of California, San Diego
La Jolla, California 92093

Statement of Work

Random variables arising in communications, radar, photodetection, and signal processing often have moment generating functions, characteristic functions, or probability generating functions for which formal mathematical expressions are readily derived theoretically. Determining the probability distributions of these variables from generating functions analytically is seldom possible. The cumulative distribution of such a variable, important because it provides false-alarm, detection, and error probabilities, can be expressed as a contour integral in the complex plane whose integrand involves the generating function. It has been found that the distribution can be accurately computed numerically if the contour is taken through a saddlepoint of the entire integrand. We propose a thorough study of the potentialities of this method of saddlepoint integration for distributions of both continuous and discrete random variables of importance in the above-mentioned fields. When the random variable results from a quadratic functional of a Gaussian random process, the generating function involves the Fredholm determinant of the autocovariance function of the process. Its calculation for points on the contour of integration by integrating vector Riccati equations will be investigated for processes that can be modeled as the output of a linear system driven by white noise. A coherent signal component of the input process can also be handled by this analysis. Acceleration of the convergence of the numerical integration by optimum choice of the contour will be examined.

Particular applications treated in the proposal are to the detectability of fading radar echoes, the distribution of the average power of a Gaussian random process, the performance of the optimum and threshold detectors of a narrow-band Gaussian stochastic signal in white noise, the distribution of the number of photoelectrons counted when a mixture of coherent and incoherent light falls on an emissive surface, and the distribution of the number of output electrons from an avalanche photodiode. Still other applications will be considered if time and resources permit.

1. Introduction

Let x be a continuous random variable with probability density function (p.d.f.) p(x) and moment generating function (m.g.f.)

$$h(u) = E(e^{-ux}) = \int_{-\infty}^{\infty} p(x)\, e^{-ux} dx. \tag{1.1}$$

Then the p.d.f. p(x) can be recovered by the inverse Laplace transform

$$p(x) = \int_{c-i\infty}^{c+i\infty} h(u)\, e^{ux}\, du/2\pi i, \tag{1.2}$$

in which the contour of integration runs parallel to the imaginary axis and lies in a strip containing the origin, but no singularities of h(u). In many problems in communications and signal processing the m.g.f. h(u) is readily determined theoretically, but calculating the p.d.f. p(x) from it analytically may be difficult or impossible. It is usually the cumulative distribution (c.d.)

$$q^{-}(x) = \int_{-\infty}^{x} p(x')\, dx' \tag{1.3}$$

or the complementary cumulative distribution (c.c.d.)

$$q^{+}(x) = 1 - q^{-}(x) = \int_{x}^{\infty} p(x')\, dx' \tag{1.4}$$

that is of interest, for these determine quantities such as the false-alarm and detection probabilities, or the average error probabilities in a communication system. The necessity of integrating p(x) enhances the complexity of the problem. We call $q^{-}(x)$ and $q^{+}(x)$ the "tail probabilities" and concentrate on calculating the former for $x < E(x)$ and the latter for $x > E(x)$, where E(x) stands for the expected value of the random variable x. They are given in terms of the

m.g.f. h(u) by the contour integrals

$$q^-(x) = \int_{c-i\infty}^{c+i\infty} u^{-1}\, h(u)\, e^{ux}\, du/2\pi i, \qquad c > 0, \tag{1.5}$$

$$q^+(x) = -\int_{c-i\infty}^{c+i\infty} u^{-1}\, h(u)\, e^{ux}\, du/2\pi i, \quad c < 0. \tag{1.6}$$

The principal purpose of this research is to investigate methods of computing the tail probabilities $q^-(x)$ and $q^+(x)$ by numerical integration of (1.5) and (1.6) along a suitable contour. Ideally one would like to integrate along that contour on which the magnitude of the integrand decreases most rapidly from its value at the point Im u = 0 as the point u moves away from the real axis in the u-plane, for then the number of steps required would be minimum [1]. This contour is known as the path of steepest descent, and along it the integrand is real, or equivalently the imaginary part Im $\Phi(u)$ of its "phase"

$$\Phi(u) = \ln h(u) + ux - \ln (\pm u) \tag{1.7}$$

vanishes. (Here $(\pm u) = -u$ when (1.6) is being integrated and $(\pm u) = u$ when (1.5) is being integrated.) This contour crosses the real u-axis at a saddlepoint $u = u_0$ of the integrand, which is determined by the equation

$$\Phi'(u) = \frac{h'(u)}{h(u)} + x - u^{-1} = 0, \qquad u = u_0 \tag{1.8}$$

(Primes stand for derivatives.) One such saddlepoint, $u_0 = u_0^-$, lies between the rightmost singularity of h(u) in Re u < 0 and the point u = 0; another, $u_0 = u_0^+$, lies to right of the origin, but to the left of any singularities on Re u > 0. When (1.5) is being integrated, the contour of integration passes through u_0^+; when (1.6) is being integrated, it passes through u_0^-. When the second derivative $\Phi''(u)$ of the phase is easily calculated, (1.8) can be expeditiously solved by Newton's method. Otherwise one can use the secant method, which estimates the second derivative by computing $\Phi'(u)$ at two close points. An alternative method for determining the saddlepoint is to solve the equation

$$\text{Im } \Phi(u_0 + i\epsilon) = 0 \tag{1.9}$$

by Newton's method or the secant method for a sufficiently small value of ϵ. It is unnecessary to determine the saddlepoint with high precision.

To trace the path of steepest descent exactly would, however, much protract the numerical integration. When the singularities of the integrand all lie on or near the real u-axis, the path of steepest descent often has approximately a parabolic form, and the contour integrals can be efficiently evaluated by taking them instead along the osculatory parabola, that is, along a parabola passing through the saddlepoint u_0, lying symmetrically about the real u-axis, and having at the saddlepoint the same curvature κ as the path of steepest descent, which is given by [1]

$$\kappa = \frac{1}{3}\, \Phi'''(u_o)/\Phi''(u_0). \tag{1.10}$$

The c.d. and the c.c.d. are then given by integrals of the form

$$q^{\pm}(x) = \int_0^{\infty} \text{Rl}[(h(u)\, e^{ux}\, (\mp u)^{-1}\, (1 - i\kappa y)]dy/\pi,$$
$$u = u_0 + \tfrac{1}{2}\, \kappa y^2 + iy, \tag{1.11}$$

with $u_0 = u_0^+$ for $q^-(x)$ and $u_0 = u_0^-$ for $q^+(x)$, and for reasons given in [2] this has been evaluated by the trapezoidal rule. One takes an initial step size of the order of $[\Phi''(u_0)]^{-1/2}$, halving the step size and repeating the numerical integration until the value of the probability stabilizes within the number of significant figures desired.

If, on the other hand, the integrand also possesses singularities above and below the real u-axis, and the path of steepest descent consequently possesses many branches, it may not be feasible to integrate along other than a straight line, possibly vertical, possibly inclined at a suitable angle to the vertical.

In what follows we shall describe our progress in this investigation, treating in Sec. 2 the evaluation of radar detection probabilities and in Sec. 3 the

calculation of the cumulative distribution of the average power in a Gaussian random process. Similar methods can be used for computing the cumulative distribution of a positive integer-valued random variable, and these are described in Sec. 4 and applied to distributions of the number of electrons at the output of a photomultiplier.

2. Quadratic Detection of Radar Signals.

(a) Signals of Fixed or Random Strength

The input to a radar receiver is passed through a filter matched to the shape of the expected echo signal, and the output of the filter is applied to a quadratic rectifier. The noise in the input is white and Gaussian; echoes from a target may also be present. The sampled outputs of the rectifier in a particular range bin are summed in M successive interpulse intervals to produce a detection statistic of the form

$$Z = \tfrac{1}{2} \sum_{j=1}^{M} r_j^2, \tag{2.1}$$

where r_j^2 is the output of the rectifier in the j-th interval. When suitably normalized, Z has a chi-squared distribution with 2M degrees of freedom under hypothesis H_0 that no signal is present; its moment generating function (m.g.f.) is

$$h_0(u) = E(e^{-uZ} \mid H_0) = (1 + u)^{-M}. \tag{2.2}$$

Under hypothesis H_1 that a target is present, an echo is received in the j-th interval with energy E_j and signal-to-noise ratio $d_j^2 = 2E_j/N$, $1 \leq j \leq M$, where N is the unilateral spectral density of the white-noise background. Then the m.g.f. of Z is

$$\begin{aligned} h_1(u) &= E(e^{-uZ} \mid H_1) = (1 + u)^{-M} \exp\left(-\frac{Su}{1 + u}\right), \\ S &= \tfrac{1}{2} D^2 = \tfrac{1}{2} \sum_{k=1}^{M} d_k^2 = E_T/N, \end{aligned} \tag{2.3}$$

where E_T is the total received energy. The probability Q_d of detection is given by the M-th order Q-function,

$$Q_d = \Pr(Z > Z_0 \mid H_1) = Q_M(D, \sqrt{2Z_0}), \tag{2.4}$$

where Z_0 is the decision level with which the statistic Z is compared [3, pp. 215-219]. The false-alarm probability

$$Q_0 = Q_M(0, \sqrt{2Z_0}) \tag{2.5}$$

can be expressed in terms of the incomplete gamma function. A saddlepoint approximation was applied in [4] to the calculation of the decision level Z_0 and the probability Q_d of detection for large numbers M of pulses integrated; typical results are tabulated there and compared with the exact probabilities.

When the radar echoes fade, the distribution of the statistic Z must be averaged with respect to the distribution of signal amplitudes. It is simplest to average the m.g.f. in (2.3) and invert it to calculate the cumulative distribution of Z and thence the average probability of detection. Four typical distributions of the fading amplitudes were enounced by Swerling [5], and we list them here with the resulting m.g.f.'s of Z:

Case I: $D = AD_0$, where A has a Rayleigh distribution,

$$p(A) = (A/A_0^2) \exp(-A^2/2A_0^2), \qquad A > 0, \tag{2.6}$$

yields the m.g.f.

$$\begin{aligned} h_1(u) &= (1+u)^{-(M-1)}[1 + (B_1+1)u]^{-1} \\ B_1 &= \tfrac{1}{2}\langle D^2\rangle = E_T/N, \end{aligned} \tag{2.7}$$

$\langle\cdot\rangle$ indicating an average with respect to the distribution of signal amplitudes.

Case II: $d_j = A_j d_0$, $\forall j$, where the A_j are statistically independent and have Rayleigh distributions like that in (2.6), yields the m.g.f.

$$h_2(u) = [1 + (1 + B_2)u]^{-M},$$
$$B_2 = 1/2 \ \langle d_j^2 \rangle = \langle E_j \rangle / N = B_1 / M. \tag{2.8}$$

The distribution of the statistic Z is a scaled chi-squared distribution with 2M degrees of freedom.

Case III: $D = AD_0$, where A has the density function

$$p(A) = (A^3/2A_0^2) \exp(-A^2/2A_0^2), \quad A > 0, \tag{2.9}$$

yields the m.g.f.

$$h_3(u) = (1 + u)^{-(M-2)}[1 + (1 + B_3)u]^{-2},$$
$$B_3 = 1/4 \ \langle D^2 \rangle = \langle E_T \rangle / 2N. \tag{2.10}$$

Case IV: $d_j = A_j d_0$, $\forall j$, where the A_j are statistically independent and have the distribution of Case III, yields the m.g.f.

$$h_4(u) = (1 + u)^M[1 + [1 + B_4)u]^{-2M},$$
$$B_4 = 1/4 \ \langle d_j^2 \rangle = \langle E_j \rangle / 2N = B_3 / M. \tag{2.11}$$

The distributions of the sum Z arising from these "Swerling cases" are given by di Franco and Rubin [6, ch. 11]. For cases III and IV the cumulative distributions are quite complicated, involving hypergeometric functions of orders depending on M. For case IV, for instance, calculating the detection probability Q_d requires summing M terms, each containing an incomplete gamma-function of order $M + k - 1$, $0 < k \leq M$.

In general, if

$$G(u) = E(e^{-Su}) = \int_0^\infty p(S)\, e^{-uS}\, dS \tag{2.12}$$

is the m.g.f. of the positive-valued random variable S, representing the total strength of the fading echoes, the m.g.f. of the random variable Z in (2.1) is, by (2.3),

$$h(u) = (1 + u)^{-M}\, G\left(\frac{u}{1 + u}\right) . \tag{2.13}$$

Its singularities will always lie in the left halfplane. In particular, if the signal strength has a gamma distribution, of which Swerling's cases I - IV are special instances,

$$p(S) = [\Gamma(k)]^{-1}\, (k/\bar{S})^k\, S^{k-1}\, e^{-kS/\bar{S}}, \tag{2.14}$$

where $\bar{S}$ is the mean total signal-to-noise ratio, then

$$G(u) = \left(1 + \frac{\bar{S}u}{k}\right)^{-k} \tag{2.15}$$

and the m.g.f. of Z is

$$h(u) = (1 + u)^{k-M}\, (1 + bu)^{-k}, \qquad b = 1 + \bar{S}/k. \tag{2.16}$$

For cases I - IV, k = 1, M, 2, 2M respectively.

The method of integration along a parabolic contour, as in (1.11), has been successfully applied to evaluating the tail probabilities for both unfading signals and signals having random strengths described by distributions p(S) of the form in (2.14). A bound has been derived for the truncation error incurred by cutting off the integration in (1.11) at a finite value of y. In most instances it suffices to stop the numerical integration when the absolute value of the integrand falls below a fraction ε of the accumulated sum times the step size Δy, whereupon the relative truncation error will be less than ε. The number of steps of numerical integration required to attain a certain accuracy is more

or less independent of the number M of signals processed by the radar receiver.

(b) Detection in Noise of Unknown Level

When the radar is being jammed by a transmitter of Gaussian noise spread over a frequency band much wider than that of the target echoes, the receiver is faced with the problem of detecting them in noise of unknown and random spectral density. A strategem that is often adopted utilizes K samples $r_j'^2$ of the quadratically rectified output of a narrowband pass filter tuned to the same frequency as that of the echoes, or to a nearby frequency; these samples are taken at times when no signals are expected to be present, and it is presumed that they have the same probability distribution as the noise components of the terms r_j^2 in (2.1). The strength of that noise is then, within an inessential constant of proportionality, estimated by the value of the statistic

$$Z' = 1/2 \sum_{j=1}^{K} r_j'^2. \tag{2.17}$$

When these samples $r_j'^2$ indeed represent noise alone, the statistic Z′ has a scaled chi-squared distribution with 2K degrees of freedom and is independent of Z in (2.1). The decision level with which the statistic Z is compared in order to decide whether any radar echo is present is made proportional to Z′, or equivalently, the receiver forms the statistic

$$X = Z - \beta Z', \tag{2.18}$$

and it decides that a signal is present whenever $X > 0$. The constant β is selected to achieve a pre-assigned false-alarm probability

$$Q_0(\beta) = \Pr (X > 0 | H_0), \tag{2.19}$$

and one wishes to calculate the probability

$$Q_d(\beta;\ S) = Pr\ (X > 0 |\ H_1) \qquad (2.20)$$

of detecting a sequence of M radar echoes of total signal-to-noise ratio S.

If the signal to be detected has a fixed, known strength, as in (2.3), the statistic X has the m.g.f.

$$\eta(u) = E(e^{-ux}) = (1 + u)^{-M}(1 - \beta u)^{-K} \exp\left(-\frac{Su}{1 + u}\right) \qquad (2.21)$$

with S the signal-to-noise ratio defined in (2.3). The probability of detection is then given by

$$Q_d(\beta;\ S) = \int_{C_-} (1 + u)^{-M}(1 - \beta u)^{-K} \exp\left(-\frac{Su}{1 + u}\right) \frac{du}{2\pi i}, \qquad (2.22)$$

where C_- is a contour parallel to the imaginary u-axis and passing between the origin and the essential singularity of the integrand at $u = -1$. One evaluates (2.22) when the signal strength S is so small that the expected value of $X = Z - \beta Z'$ is negative; here

$$E(X) = S + M - \beta K. \qquad (2.23)$$

When $E(X) > 0$, on the other hand, one evaluates

$$1 - Q_d(\beta;\ S) = \int_{C_+} (1+ u)^{-M}(1 - \beta u)^{-K} \exp\left(-\frac{Su}{1 + u}\right) \frac{du}{2\pi i} \qquad (2.24)$$

along a contour lying in $0 < \mathrm{Re}\ u < 1/\beta$.

The prescription, "Choose the alternative hypothesis H_1 when $X = Z - \beta Z' > 0$," is equivalent to the F-test of the analysis of variance, and the F-statistic is

$$F = KZ/MZ'. \tag{2.25}$$

The false-alarm probability $Q_0(\beta)$ is related to the central F-distribution, and the detection probability $Q_0(\beta; S)$ to the noncentral F-distribution, the signal-to-noise ratio S playing the role of the noncentrality parameter. In [7] the computation of the noncentral F-distribution by integrating (2.22) or (2.24) numerically along a straight vertical contour was treated, and a bound on the error incurred by truncating the range of numerical integration was presented. It was shown that the simple rule that the summation be stopped when the absolute value of the integrand falls below a fraction ϵ of the accumulated sum times the step size Δy suffices to bound the relative error in the computed probability within that same fraction ϵ.

If the radar echoes are fading as described in part (a), the average detection probability is obtained by averaging the integrals in (2.22) and (2.24) with respect to S,

$$Q_d(\beta; \bar{S}) = \int_{C_-} (1 + u)^{-M}(1 - \beta u)^{-K} G\left(\frac{u}{1 + u}\right) \frac{du}{2\pi i}, \tag{2.26}$$

$$1 - Q_d(\beta; \bar{S}) = \int_{C_+} (1 + u)^{-M}(1 - \beta u)^{-K} G\left(\frac{u}{1 + u}\right) \frac{du}{2\pi i}, \tag{2.27}$$

where $\bar{S}$ is the average total signal-to-noise ratio and G(u) is the m.g.f. of the distribution of the random signal-to-noise ratio S, as in (2.12). Again it is possible to evaluate these probabilities by numerical integration along a vertical straight line or other suitable contour. Bounds on the truncation error when the m.g.f. is given as in (2.15) have been determined and will be presented in a paper under preparation.

3. The Average Power of a Random Process

We seek the probability distribution of the average power

$$V = T^{-1} \int_0^T [z(t)]^2 \, dt \tag{3.1}$$

of a Gaussian random process

$$z(t) = x(t) + s(t), \qquad 0 < t < T, \tag{3.2}$$

in which $x(t)$ is a stationary Gaussian random process of mean zero and autocovariance function

$$\phi(t - s) = E[x(t)\, x(s)], \tag{3.3}$$

and $s(t)$ is a deterministic signal. This problem was first treated by Slepian [8], who assumed $s(t) = 0$; references to other work are given in the proposal [9]. Our approach is to calculate the cumulative distribution $q^-(x) = \Pr(V < x)$ and its complement $q^+(x) = \Pr(V > x)$ by numerical integration of the contour integrals

$$q^-(x) = \int_{C^+} u^{-1} h(u)\, e^{ux} \, du/2\pi i, \tag{3.4}$$

$$q^+(x) = -\int_{C_-} u^{-1} h(u)\, e^{ux} \, du/2\pi i, \tag{3.5}$$

where C_- and C_+ are suitable contours obtained by deforming the straight vertical contours in (1.5) and (1.6). The contours pass to the right of any singularities of the moment-generating function (m.g.f.) $h(u)$, which in this problem lie on the

negative real axis of the u-plane. The contour C_- lies to the left of the origin, C_+ to the right.

The moment-generating function

$$h(u) = E(e^{-uV}) \tag{3.6}$$

of the random variable V was shown in the proposal [9] to be given by

$$h(u) = [D(2u/T)]^{-1/2} \exp\left[-\frac{2u}{T} J(2u/T)\right], \tag{3.7}$$

where D(u) is the Fredholm determinant

$$D(u) = \prod_{j=1}^{\infty} (1 + \lambda_j u) \tag{3.8}$$

associated with the homogeneous integral equation

$$\lambda f(t) = \int_0^T \phi(t - s)\, f(s)\, ds, \tag{3.9}$$

whose kernel is the autocovariance function $\phi(t - s)$ and whose eigenvalues λ are denoted by $\lambda_1, \lambda_2, \ldots$. The function J(u) is given by

$$J(u) = 1/2 \sum_{j=1}^{\infty} \frac{s_j^2}{1 + \lambda_j u}, \tag{3.10}$$

where

$$s_j = \int_0^T s(t)\, f_j(t)\, dt \tag{3.11}$$

are the coefficients of a Fourier series for the signal s(t) in terms of the eigenfunctions $f_j(t)$ of (3.9). As indicated in the proposal [9],

$$D(u) = \exp \int_0^T h(t, t; u; t)\, dt \tag{3.12}$$

in terms of the solution $h(r, t; u; \tau)$ of the integral equation

$$h(r, t; u; \tau) + u \int_0^\tau \phi(r - v)\, h(v, t; u; \tau)\, dv = u\phi(r - t), \qquad 0 < (r, t) < \tau, \tag{3.13}$$

and

$$J(u) = 1/2 \int_0^T [s(t) - \sigma(t; u)]^2\, dt \tag{3.14}$$

with

$$\sigma(t; u) = \int_0^t h(t, v; u; t)\, s(v)\, dv. \tag{3.15}$$

(a) Application to RLC Noise

In order to test various methods of calculating the m.g.f. $h(u)$ needed in (3.4) and (3.5) and of carrying out the subsequent numerical evaluation of those contour integrals, we took the process $z(t) = x(t)$ to be Gaussian RLC noise of spectral density

$$S(\omega) = \frac{4\mu\omega^2}{(\omega^2 - \omega_0^2)^2 + 4\mu^2\omega^2} \tag{3.16}$$

and unit variance, for which the autocovariance function is

$$\phi(s) = (\eta_1 - \eta_2)^{-1} [\eta_1 \exp(-\eta_1 |s|) - \eta_2 \exp(-\eta_2 |s|)], \tag{3.17}$$

with

$$\eta_1 = \mu + (\mu^2 - \omega_0^2)^{1/2}, \quad \eta_2 = \mu - (\mu^2 - \omega_0^2)^{1/2}. \tag{3.18}$$

The signal $s(t)$ was assumed zero. For this process the m.g.f. $h(u)$ was worked

out by Slepian [8] and can be written

$$
\begin{aligned}
h(u) &= e^{r}(A^2 - B^2)^{-1/2}, \\
A &= [(g+1)^2 e^{rg} - (g-1)^2 e^{-rg}]/4g, \\
B &= v(e^{rg'} - e^{-rg'})/4g', \\
v &= 2u/r, \qquad r = \mu T = \omega_0 T/2Q, \\
g &= (1-v)^{1/2}, \qquad g' = (1-v-4Q^2)^{1/2},
\end{aligned}
\tag{3.19}
$$

with Q the usual quality factor of the RLC circuit, $Q = \omega_0/2\mu$.

The cumulative distributions for the average power V of this RLC noise were computed for various values of $r = \mu T$ and Q and are plotted in Figs. 1 and 2. The contours C_+ and C_- were, as discussed in Sec. 1, taken as parabolas passing through saddlepoints u_0^+ and u_0^-, respectively; $u_0^+ > 0$, and $u_0^- < 0$, u_0^- lying to the right of the leftmost singularity of the m.g.f. h(u). The integral in (1.11) was evaluated by the trapezoidal rule. The size of the segments Δy into which the integration variable y is divided was taken initially as

$$\Delta y = [2\Phi''(u_0)]^{-1/2}, \tag{3.20}$$

and it was successively halved until the value of the integral ceased changing in the number of significant figures sought. The integration was stopped when the absolute value of the integrand fell below 10^{-7} times Δy times the accumulated sum.

The method used here has the advantage over Slepian's [8] of not requiring prior computation of the eigenvalues λ of (2.9); for a large time-bandwidth product $r = \mu T$ the number of significant eigenvalues λ is of the order of r and also large, and Slepian's method entails an overlong computation. In ours the number of steps of numerical integration remains of roughly the same order of

magnitude over the entire range of values of $r = \mu T$.

The results plotted in Figs. 1 and 2 show that the distribution of V is insensitive to the value of Q unless $r = \mu T$ is of the order of 1 or less. For $r = 4$ and $r = 8$ the curves for $Q = 0$ and $Q = \infty$ lie so close that curves for intermediate values of Q could not be exhibited.

(b) Kreĭn-Levinson Method

When, as we assume in this report, the noise process x(t) is stationary, the functions D(u) and J(u) needed for the m.g.f. in (3.7) can in principle be calculated by the Kreĭn-Levinson method described by Kailath et al. [10], and we have begun to investigate this possibility.

We define

$$A_u(\tau, r) = h(\tau, r; u; \tau) \tag{3.21}$$

in terms of the solution of (3.13). It obeys the integral equation

$$A_u(\tau, r) + u\int_0^\tau A_u(\tau, v)\ \phi(v - r)\ dv = u\phi(\tau - r), \qquad 0 < r < \tau, \tag{3.22}$$

which is obtained by setting $t = \tau$ in (3.13) and using

$$h(r, t; u; \tau) = h(t, r; u; \tau).$$

In terms of this function, (3.12) and (3.15) become

$$D(u) = \exp\int_0^T A_u(t, t)\ dt, \tag{3.23}$$

$$\sigma(t; u) = \int_0^t A_u(t, v)\ s(v)\ dv. \tag{3.24}$$

As shown in [10], this function $A_u(t, r)$ obeys the Sobolev identity

$$\left(\frac{\partial}{\partial t} + \frac{\partial}{\partial r}\right) A_u(t, r) = -A_u(t, 0)\, A_u(t; t - r), \tag{3.25}$$

and that paper suggests solving (3.22) by a numerical method based on this identity and on the equation (3.22) with $r = 0$,

$$A_u(t, 0) + u\int_0^t A_u(t, v)\, \phi(v)\, dv = u\phi(t). \tag{3.26}$$

Taking small steps of size Δ in the variables t and r, one writes these approximately as

$$A_u(\overline{k+1}\Delta, \overline{j+1}\Delta) = A_u(k\Delta, j\Delta) - \Delta A_u(k\Delta, 0) A_u(k\Delta, \overline{k-j}\Delta) \tag{3.27}$$

and

$$A_u(k\Delta, 0) = u\phi(k\Delta) - u\Delta \sum_{j=1}^{k} A_u(k\Delta, j\Delta)\, \phi(j\Delta). \tag{3.28}$$

Starting with the initial condition

$$A_u(0, 0) = u\phi(0) = u, \tag{3.29}$$

one determines $A_u(\Delta, \Delta)$ from (3.27) and then $A_u(\Delta, 0)$ from (3.28). Continuing, one has at stage k the values of $A_u(k\Delta, j\Delta)$, $0 \leq j \leq k$, and uses them in (3.27) to compute $A_u(\overline{k+1}\Delta, \overline{j+1}\Delta)$, $0 \leq j \leq k$. These are then used in (3.28), with k replaced by k+1, to determine $A_u(\overline{k+1}\Delta, 0)$. This method goes by the name of the "Kreĭn-Levinson algorithm" [10]. The integrals in (3.23), (3.24), and (3.14), replaced by numerical quadrature formulas, can be used simultaneously to compute D(u) and J(u). This whole computation is carried out for each point u on the contour of integration, which we are taking to be the parabola figuring in (1.11).

This algorithm was tried for RLC noise, and it was found inaccurate even when the interval (0, T) was divided into one hundred steps, $\Delta = 0.01T$. The

approximation of (3.25) by (3.27) is simply too crude. Improved accuracy, yet with fewer subintervals Δ, resulted from replacing the integral equation (3.22) by its approximation by the trapezoidal rule,

$$A_u(k\Delta, i\Delta) + u\Delta \left[\frac{1}{2} A_u(k\Delta, 0)\ \phi(i\Delta) + \sum_{j=1}^{k-1} A_u(k\Delta, j\Delta)\ \phi(\overline{i-j}\Delta) + \frac{1}{2} A_u(k\Delta, k\Delta)\ \phi(\overline{k-i}\Delta)\right] = u\ \phi(\overline{k-i}\Delta) \tag{3.30}$$

which constitutes a set of $(k + 1)$ linear simultaneous equations for $A_u(k\Delta, i\Delta)$, $0 \leq i \leq k$. These were solved approximately by three iterations of the conjugate-gradient method [11], starting with an approximate solution obtained from (3.27) and (3.28).

In order to evaluate the contour integral (1.11) by numerical integration along a parabolic contour through the saddlepoint u_0, it is necessary first to find the saddlepoint by solving (1.8) for $u = u_0$ and then to calculate the curvature κ from (1.10), and this entails computing the first three derivatives of the phase $\Phi(u)$ of (1.7) with respect to u and evaluating them at the saddlepoint u_0, which is real. In order to avoid the iteration involved in solving (1.8) for $u = u_0$, we picked the value of u_0 at the start and used (1.8) to determine the corresponding value of the level $V = x$ at which the cumulative distribution or its complement is evaluated.

From (3.7), (1.7), and (3.23) the phase of the integrand is

$$\Phi(u) = D(2u/T) + ux - \ln(\pm u) = \int_0^T A_{u'}(t, t)\, dt + ux - \ln(\pm u),\ u' = 2u/T. \tag{3.31}$$

The derivatives of the phase $\Phi(u)$, therefore, involve the partial derivatives of $A_u(t, r)$ with respect to the real parameter u, and these partial derivatives of

$A_u(t, r)$ obey integral equations obtained by differentiating (3.22) with respect to u. The Sobolev identity (3.25) can likewise be differentiated with respect to u. The resulting integral equations for the partial derivatives of $A_u(t, r)$, $u = u_0$, were also solved by the conjugate-gradient method, using the derivatives of (3.27) and (3.28) with respect to u to provide starting values. Because the second and third derivatives are not needed to great accuracy, fewer iterations of the conjugate-gradient algorithm suffice.

This scheme succeeded quite satisfactorily, but further study and refinement are necessary. The solution $A_u(\tau, r)$ of (3.22) contains a term of the form $u(1 + \tau u)^{-1}$, $0 < r < \tau$, which dominates when $\mu\tau \ll 1$, μ the damping constant in (3.16-.18). When the imaginary part of u is large, that is, when the point u is far out on the parabolic contour of integration, this term results in a rapid initial gyration of the solution as a function of τ, and this cannot be accurately followed by the numerical algorithm unless very small step sizes Δ are utilized. The ensuing inaccuracy is not serious, for the value of the integrand of (1.11) is by then quite small. Nevertheless, an attempt will be made to subtract this term from $A_u(\tau, r)$ at the beginning and to solve only for the residual portion of that function numerically.

(c) Chandrasekhar Equations

Alternative methods of computing the m.g.f. h(u) are available when the process x(t) can be considered as the output of a linear system driven by white noise. Under our continuing assumption that the process x(t) is stationary, the system can be taken as time invariant and to be in the steady state. It is then necessary to know an $n \times n$ dynamical matrix $\underset{\sim}{E}$, an n-element column vector $\underset{\sim}{c}$, and an n-element row vector $\underset{\sim}{c}$ such that the process can be represented as

$$x(t) = \underset{\sim}{c}\, \underset{\sim}{x}(t) \tag{3.32}$$

with

$$\frac{d\underset{\sim}{x}}{dt} = \underset{\sim}{F}\underset{\sim}{x} + \underset{\sim}{G}\, w(t), \tag{3.33}$$

where $\underset{\sim}{x}$ is an n-element state vector and w(t) is white Gaussian noise with spectral density R. The steady-state variance equation

$$\underset{\sim}{F}\underset{\sim}{\Lambda} + \underset{\sim}{\Lambda}\underset{\sim}{F}^{+} + R\,\underset{\sim}{G}\underset{\sim}{G}^{+} = 0 \tag{3.34}$$

is solved for the steady-state variance matrix $\underset{\sim}{\Lambda}$, and the known value of

$$\phi(0) = \underset{\sim}{C}\underset{\sim}{\Lambda}\underset{\sim}{C}^{+} \tag{3.35}$$

establishes the required value of R.

As indicated in the proposal [9], the Fredholm determinant D(u) can be calculated from the solution $\underset{\sim}{\xi}_u$ of the matrix Riccati equation

$$\frac{d\underset{\sim}{\xi}_u}{dt} = \underset{\sim}{F}\underset{\sim}{\xi}_u + \underset{\sim}{\xi}_u\underset{\sim}{F}^{+} - \underset{\sim}{\xi}_u\underset{\sim}{C}^{+}\underset{\sim}{C}\underset{\sim}{\xi}_u + u\, R\underset{\sim}{G}\underset{\sim}{G}^{+}, \qquad 0 < t < T, \tag{3.36}$$

with initial condition

$$\underset{\sim}{\xi}_u(0) = u\underset{\sim}{\Lambda}(0); \tag{3.37}$$

u is in general a complex variable and stands for a point on the contour of integration. Then

$$D(u) = \exp\left[\int_0^T \underset{\sim}{C}\underset{\sim}{\xi}_u(t)\ \underset{\sim}{C}^{+}\, dt\right]. \tag{3.38}$$

Furthermore, the function $\sigma(t; u)$ in (3.14) is given by

$$\sigma(t; u) = \underset{\sim}{C}\underset{\sim}{\xi}_u(t), \tag{3.39}$$

where $\hat{\underset{\sim}{s}}_u(t)$ is the solution of the vector differential equation

$$\frac{d\hat{\underset{\sim}{s}}_u}{dt} = \underset{\sim}{F}\hat{\underset{\sim}{s}}_u + \underset{\sim}{\xi}_u(t)\,\underset{\sim}{C}^+[s(t) - \sigma(t;\, u)] \tag{3.40}$$

in terms of the solution of (3.36).

The RLC noise treated in part (a) can be generated by a second-order system with dynamical matrix

$$\underset{\sim}{F} = \begin{bmatrix} -2\mu & -\omega_0^2 \\ 1 & 0 \end{bmatrix} \tag{3.41}$$

and with

$$\underset{\sim}{G} = \begin{bmatrix} 1 \\ 0 \end{bmatrix}, \qquad \underset{\sim}{C} = (1 \quad 0). \tag{3.42}$$

The matrix $\underset{\sim}{\xi}_u$ is then ordinarily 2×2, but when as here u is complex and one wishes to use standard routines for solving systems of first-order differential equations, it is necessary to consider the real and imaginary parts of the four elements of $\underset{\sim}{\xi}_u(t)$ separately, and six first-order differential equations for the distinct elements of this complex matrix need to be solved. Simultaneously, (3.38) is integrated after conversion to a differential equation,

$$\frac{dE}{dt} = \underset{\sim}{C}\underset{\sim}{\xi}_u(t)\,\underset{\sim}{C}^+ \qquad 0 < t < T, \qquad E(0) = 0, \tag{3.43}$$

$$D(u) = \exp E(T). \tag{3.44}$$

Since E(t) is also complex, this adds two more equations, making eight in all. In general, for an n-th order system, the number of differential equations to be integrated amounts to $n^2 + n + 2$.

By using the DVERK routine in the IMSL Library of computer routines we were able to integrate the Riccati equation (3.36) along with (3.43), and we obtained values of the Fredholm determinant D(u) in agreement with those calculated from

(3.19) directly. Somewhat cumbersome precautions had to be taken, however, to ensure that the initial steps Δt in the time variable were small enough to maintain stability.

For this reason we turned instead to the so-called Chandrasekhar equations. As shown by Kailath [12], the matrix Riccati equation can be replaced by the vector equations

$$\frac{d\underset{\sim}{K}_u}{dt} = -\underset{\sim}{Y}_u \underset{\sim}{Y}_u^+ \underset{\sim}{C}^+, \tag{3.45}$$

$$\frac{d\underset{\sim}{Y}_u}{dt} = (\underset{\sim}{F} - \underset{\sim}{K}_u \underset{\sim}{C})\ \underset{\sim}{Y}_u, \tag{3.46}$$

with initial conditions

$$\underset{\sim}{K}_u(0) = \underset{\sim}{Y}_u(0) = u\underset{\approx}{\Lambda}\underset{\sim}{C}^+. \tag{3.47}$$

When u is complex, and we include the two differential equations arising from (3.43),

$$\frac{dE}{dt} = \underset{\sim}{C}\underset{\sim}{K}_u(t), \qquad E(0) = 0, \tag{3.48}$$

the Chandrasekhar method requires solving $4n + 2$ first-order differential equations, which amount for a second-order system to ten instead of eight as with the matrix Riccati equation. For a third-order system both methods require solving fourteen equations, and for $n > 3$ the Chandrasekhar method involves fewer equations than the Riccati method.

When we tried the Chandrasekhar method for RLC noise, instability arose only when the imaginary part of the complex parameter u was large, that is, at points far out on the parabolic contour of integration in (1.11). This appears to be related to the term $u(1 + \tau u)^{-1}$ that causes an initial sharp gyration in the function $A_u(\tau, r)$ treated in part (b). Indeed, $A_u(\tau, \tau) = \underset{\sim}{C}\ \underset{\sim}{K}_u(\tau)$, $0 < \tau < T$.

We shall have to investigate whether it is possible to subtract out what corresponds to that term in order to make the Chandrasekhar method also efficient for all values of u at which the function D(u) is needed.

Since (3.40) depends on $\underset{\sim}{\xi}_u$ only through $\underset{\sim}{K}_u = \underset{\sim}{\xi}_u \underset{\sim}{C}^+$, the Chandrasekhar method will also suffice for calculating the function J(u) in (2.7) and hence can be applied even when the process z(t) contains a deterministic signal s(t), but this has not yet been studied.

The derivatives of the phase $\Phi(u)$ of the integrands of (3.4) and (3.5), defined as in (1.7), can also be calculated by the Chandrasekhar method. The necessary equations are obtained by differentiating (3.45), (3.46), and (3.48) with respect to u. These derivatives are needed only for real values of u. For RLC noise we calculated the first three derivatives of $\Phi(u)$ at the saddlepoint by integrating the fifteen simultaneous first-order differential equations that arise by this process, using them as described at the end of part (b) to determine the level $V = x$ by (1.8) and the curvature κ of the path of integration by (1.10). The results agreed well with those calculated by the exact m.g.f. in (3.19). A detailed comparison of the methods of parts (b) and (c) remains to be carried out. The former requires only the autocovariance function $\phi(t - r)$ of the process x(t); for the latter a state-space model must be constructed, but standard routines for integrating systems of first-order differential equations can then be applied.

4. Photoelectron Counting Probabilities

(a) Introduction

Let x be a positive integer-valued random variable with a probability distribution

$$\Pr(x = k) = p_k, \qquad k = 0, 1, 2, \ldots,$$

cumulative distribution (c.d.)

$$Q_n^- = \Pr(x < n) = \sum_{k=0}^{n-1} p_k, \tag{4.1}$$

and complementary cumulative distribution (c.c.d.)

$$Q_n^+ = \Pr(x \geq n) = 1 - Q_n^- = \sum_{k=n}^{\infty} p_k. \tag{4.2}$$

In the applications we usually have in mind, x is the number of electrons counted during a specific interval (0, T) at the output of some photoelectric device. The c.d. and the c.c.d. can be computed from the probability generating function (p.g.f.)

$$h(z) = E(z^x) = \sum_{k=0}^{\infty} p_k z^k \tag{4.3}$$

by the contour integrals

$$Q_n^- = \int_{C_-} \frac{z^{-n}\, h(z)}{1 - z}\, \frac{dz}{2\pi i}, \tag{4.4}$$

$$Q_n^+ = \int_{C_+} \frac{z^{-n}\, h(z)}{z - 1}\, \frac{dz}{2\pi i}, \tag{4.5}$$

in which C_- and C_+ are circles centered at the origin $z = 0$; C_+ also encloses the point $z = 1$, C_- does not; and the contours enclose no singularities of the p.g.f. $h(z)$, all of which lie outside the unit circle.

As shown in [13], the numerical evaluation of these integrals is most efficient when the contours pass through saddlepoints of the integrand, that is, through points z_0 that are solutions of

$$\Psi'(z) = \frac{h'(z)}{h(z)} - \frac{n}{z} - \frac{1}{z-1} = 0, \tag{4.6}$$

where

$$\Psi(z) = \ln h(z) - n \ln z - \ln[\pm(z-1)] \tag{4.7}$$

is the "phase" of the integrands, $\pm(z-1)$ standing for $1 - z$ when (4.4) is integrated and for $z - 1$ when (4.5) is integrated. One such saddlepoint, $z_0 = \bar{z_0}$, lies in $0 < z_0 < 1$, the other lies on the real z-axis between $z = 1$ and the leftmost singularity of $h(z)$. The saddlepoint can usually be most expeditiously located by solving (4.6) by Newton's method or the secant method. Alternatively, the equivalent of (1.9) can be used.

The circular contours in (4.4) and (4.5) often suffer the disadvantage that the integrand is oscillatory along them, so that too many steps may be needed in order to obtain an accurate value of Q_n^+ or Q_n^- by numerical integration. The value of the integrand decreases most rapidly from its value at the saddlepoint when the contour is taken as the path of steepest descent through the saddlepoint. Along that path $\operatorname{Im} \Psi(z) = 0$. Determining the path of steepest descent, however, would much protract the evaluation of the contour integral. In many cases it has been found that the path of steepest descent, which lies symmetrically about the real axis, has nearly a parabolic form, and it is then expeditious to use instead its osculatory parabola, that is, a parabola passing through the saddlepoint z_0 and having the same curvature

$$\kappa = \frac{1}{3}\,\Psi'''(z_0)/\Psi''(z_0) \tag{4.8}$$

at the point $z = z_0$. (Primes indicate differentiation.) Along this parabola

$$z = z_0 + 1/2\ \kappa y^2 + iy, \tag{4.9}$$

and the integral to be evaluated numerically is

$$Q_n^{\pm} = \pi^{-1} \int_0^{\infty} \mathrm{Re}\left[\frac{h(z)\,z^{-n}}{\pm(z-1)}\,(1 - i\kappa y)\right] dy. \tag{4.10}$$

The initial step size is taken as

$$\Delta y = [\Psi''(z_0)]^{-1/2} \tag{4.11}$$

and successively halved until the values of the probability stabilize to the number of significant figures desired. The trapezoidal rule is used for reasons described by Rice [2].

(b) Single-Stage Photomultiplication

The contour-integration method has been applied to finding the distribution of the number of electrons at the output of a photomultiplier with a single stage of multiplication [14]. Light striking a photoelectrically emissive surface ejects a number k of photoelectrons during an interval (0, T) with probability Π_k. The p.g.f. of this distribution is

$$f(z) = \sum_{k=0}^{\infty} \Pi_k z^k. \tag{4.12}$$

Each such "primary" electron is accelerated by an applied voltage, impinges on a second metallic surface, and ejects from it a random number of secondary

electrons. Let $p_m^{(s)}$ be the probability that a given primary electron ejects m secondary electrons; the p.g.f. of this distribution is

$$g(z) = \sum_{m=0}^{\infty} p_m^{(s)} z^m. \tag{4.13}$$

Then the p.g.f. of the total number of secondaries during (0, T) is

$$h(z) = \sum_{n=0}^{\infty} p_n z^n = f\big(g(z)\big), \tag{4.14}$$

where p_n is the probability that n secondary electrons appear at the output of this device.

In this work it was assumed that the distribution of the number of secondary electrons per primary has the Poisson form, so that

$$g(z) = e^{G(z-1)}, \tag{4.15}$$

where G is the gain. The output distribution can then be computed from

$$p_n = \sum_{k=1}^{\infty} \Pi_k (kG)^n \, e^{-kG}/n! \tag{4.16}$$

with cumulative distribution determined as in (4.1) by addition. Alternatively, one can use the finite relations

$$\begin{aligned} p_0 &= f(e^{-G}), \\ p_n &= G^n \sum_{k=1}^{n} f_k \, \overline{S}(n, k) \, e^{-kG}, \qquad n > 0, \end{aligned} \tag{4.17}$$

where

$$f_k = \frac{d^k}{dz^k} f(z)\Big|_{z=e^{-G}}, \tag{4.18}$$

and where $\bar{S}(n, k)$ are modified Stirling numbers of the second kind and obey the recurrent relations

$$\bar{S}(1, 1) = 1, \quad \bar{S}(k, n) = 0, \quad k > n,$$
$$\bar{S}(n + 1, k) = [\bar{S}(n, k - 1) + k\bar{S}(n, k)]/(n + 1). \tag{4.19}$$

These formulas were used to compute exact values of the probabilities Q_n^- and Q_n^+ for comparison with those computed by our approximation methods. They involve lengthy computations when the number n is large, and round-off error introduces large relative error into the c.c.d. $Q_n^+ = 1 - Q_n^-$ when Q_n^- is computed as in (4.1).

Three types of primary distribution $\{\Pi_k\}$ were treated: (i) that arising when the incident light has a Lorentz spectral density, and for which the probabilities Π_k can be calculated by a method given by Bédard [15]; (ii) the negative binomial distribution

$$\Pi_k = \frac{\Gamma(M + k)}{k!\,\Gamma(M)} (1 - v)^M v^k, \quad v = N_p/(N_p + M), \tag{4.20}$$

with N_p the mean number of primary electrons, and M the number of temporal modes or "degrees of freedom", given roughly by the product of the bandwidth W of the incident light and the duration T of the counting interval; and (iii) the Poisson distribution

$$\Pi_k = N_p^k \exp(-N_p)/k!, \tag{4.21}$$

for which the output distribution possesses the Neyman Type-A form.

For primary distributions of type (i) and, for M an integer, of type (ii), the p.g.f. f(z) possesses poles z_k lying on the positive real z-axis to the right

of $z = 1$, whereupon the output p.g.f. $h(z)$ possesses poles at the points

$$\zeta_k^{(r)} = 1 + G^{-1}(\ln z_k + 2r\pi i), \tag{4.22}$$

for all positive and negative integral values of r, including $r = 0$. The contour integral (3.5) can then be evaluated as a residue series with terms corresponding to each point of this doubly infinite lattice of poles. For the negative-binomial primary distribution, the array shrinks to a vertical column of multiple poles of order M at the points

$$\zeta_r = 1 + G^{-1}(-\ln v + 2r\pi i). \tag{4.23}$$

When the number n of output electrons is of the order of or greater than the expected value

$$E(n) = N_p G, \tag{4.24}$$

only a very few of the poles above and below the real axis contribute significantly to the residue series. The number of columns of the lattice that need to be included under case (i) (incident light with a Lorentz spectral density) is of the order of the time-bandwidth product WT. Formulas for computing the residues and numerical examples are given in [14]. Unless WT is very large, this residue method is most efficient for computing the c.c.d. Q_n^+ with $n > E(n)$.

Consideration was given to using the contour integrals in (4.4) and (4.5) for computing the c.d. and the c.c.d. of the number of output electrons. The path of steepest descent is now too complicated to be utilized or even approximated, for it consists of a number of hairpin-like curves opening to the right and passing around each of the poles of $h(z)$. We therefore used instead a straight vertical path of integration passing through the saddlepoint of the integrand lying on the real z-axis; the one lying in $0 < z < 1$ was used for Q_n^-, and the

one lying in $1 < z < \zeta_1^{(0)}$ was used for Q_n^+, these having been determined by solving (4.6) by Newton's method. A bound on the error incurred by truncating the numerical integration was worked out. Values of Q_n^- and Q_n^+ over a broad range of values of n could be accurately computed in this way without requiring more than one hundred or so steps of numerical integration. Details are given in Sec. 4 of [14]. This method does not require that the number M in (4.20) be an integer. The contour-integration method can be used for all three types of primary distribution.

On each branch of the path of steepest descent of the integrand in (4.4) and (4.5) there is a point z_k at which the magnitude of the integrand is maximum; this is a saddlepoint of the integrand. The contribution of each branch to an integration of (4.4) or (4.5) along its path of steepest descent can be crudely approximated by assuming that in the neighborhood of each saddlepoint z_k the integrand has a Gaussian form, and this leads to the formula

$$Q_n^{\pm} \simeq \sum_{k=-\infty}^{\infty} [2\pi\Psi''(z_k)]^{-1/2} \exp [\Psi(z_k)], \tag{4.25}$$

where $\Psi(z_k)$ is the phase of the integrand as in (4.7) and $\Psi''(z_k)$ is its second derivative evaluated at the k-th saddlepoint [4]. For the most part two or three saddlepoints on each side of the principal one z_0 on the real z-axis are all that it is worth taking into account; often the one at z_0 alone suffices. Improved accuracy was obtained by evaluating the contribution of the principal branch of the path of steepest descent, which crosses the real axis at z_0, by means of the uniform asymptotic expansion described in [16] and [17]. The details of this method are to be found in Sec. 5 of [14].

(c) Multistage Photomultiplier

A photomultiplier usually has not one, but several stages of electron multiplication. We number the stages, each associated with an electrode called a "dynode", from the last. A single electron striking the k-th dynode ejects n secondary electrons from it with probability $p_n^{(k)}$; the collection of these probabilities constitutes the k-th "single-stage" distribution and has a p.g.f.

$$g_k(z) = \sum_{n=0}^{\infty} p_n^{(k)} z^n. \tag{4.26}$$

Then if there are N stages in all, the probability p_n that n electrons emerge at the output when a single primary electron strikes the N-th dynode has a p.g.f.

$$H_N(z) = \sum_{m=0}^{\infty} p_m z^m, \tag{4.27}$$

where

$$\begin{aligned} H_1(z) &= g_1(z), \\ H_k(z) &= g_k\big(H_{k-1}(z)\big), \qquad k = 2, 3, \ldots, N. \end{aligned} \tag{4.28}$$

If the distribution of primary electrons again has the p.g.f. f(z) defined in (4.12), the total number of output electrons has the p.g.f. $f\big(H_N(z)\big)$.

In this study we have concentrated on calculating the cumulative output distributions, defined as in (4.1) and (4.2), for a single primary electron, so that in (4.3)-(4.5)

$$h(z) = H_N(z).$$

We assumed that all the single-stage distributions have the same negative-binomial, or Polyà form, with common p.g.f.

$$g_k(z) = g(z) = [1 - bG(z - 1)]^{-1/b}, \qquad b > 0, \tag{4.29}$$

which corresponds to the distribution in (4.20) with

$$M = 1/b, \qquad v = bG/(1 + bG).$$

Again G is the gain per stage; the overall gain of the photomultiplier is

$$G_0 = G^N, \tag{4.30}$$

where N is the number of stages. The Poisson single-stage distribution represented by (4.15) arises in the limit $b \to 0$.

The singularities of the overall p.g.f. $H_N(z)$ now lie on or close to the portion of the real z-axis lying to the right of the point $z = 1$, and the path of steepest descent has roughly the form of a parabola lying symmetrically about the real z-axis and opening to the right. This path can be replaced by its osculatory parabola, whose curvature κ at the saddlepoint is determined by (4.8). The first three derivatives of the phase $\Psi(z)$ of the integrand, defined as in (4.7), are computed by an N-fold set of three recurrent relations. The cumulative probabilities Q_n^+ are then computed by numerical integration of (4.10). The results were compared with values computed by the recurrent relations given by Prescott [18] for $N = 3$ and values of n up to 100, and the agreement was excellent. The recurrent relations require of the order of n^2 operations to compute p_n or Q_n^+, and this number is independent of the number of significant figures sought. Thus for $n = 3000$ of the order of nine million operations would be required, in contrast to the ten or twenty steps of numerical integration of (4.10) needed for adequate precision.

When the cumulative distributions Q_n^+ so calculated are plotted on a semi-logarithmic grid for various numbers N of stages of multiplication, the overall gain $G_0 = G^N$ being kept fixed, one finds the points lying closer and closer to

straight lines as N increases. The results are fitted quite closely by a geometric or "exponential" distribution,

$$\begin{aligned} p_0 &= 1 - (1 - v)G_o, \\ p_n &= G(1 - v)^2 v^{n-1}, \qquad n > 0, \\ Q_n^+ &= G_0(1 - v)v^{n-1}, \qquad n > 0, \end{aligned} \tag{4.31}$$

in which the parameter v is given by

$$v = a/(a + 1), \qquad a = \frac{\kappa_2(G_0 - 1)}{2G(G - 1)}, \tag{4.32}$$

where κ_2 is the second factorial moment of the single-stage distribution and G is the gain per stage,

$$G = g'(1), \qquad \kappa_2 = g''(1), \tag{4.33}$$

primes denoting differentiation. This value of v is chosen so that the distribution in (4.31) has the same variance as the exact distribution,

$$\text{Var } n = \frac{\sigma^2 G_0(G_0 - 1)}{G(G - 1)}, \qquad \sigma^2 = \kappa_2 + G - G^2. \tag{4.34}$$

A number of observers have reported approximately exponential distributions for the number of output electrons in photomultipliers, but an adequate explanation of this phenomenon seems to have been lacking [18]. In [19] the distribution in (4.31) was shown to approach the true output distribution under the conditions stated: the overall gain $G_0 = G^N$ is fixed, the single-stage distributions are identical, and the number N of stages increases, the gain G per stage decreasing simultaneously toward 1.

This behavior is the counterpart for multiplicative processes of the central-limit theorem for sums of independent, identically distributed random variables. If N random variables have mean zero, and one scales their sum by

multiplying by $N^{-1/2}$, the distribution of the scaled sum approaches the Gaussian form as N increases. Furthermore, if the random variables already have a Gaussian distribution, their sum has exactly a Gaussian distribution. For multiplicative processes the geometric distribution plays the same role as the Gaussian does for sums. If the single-stage distributions are geometric, with p.g.f.'s

$$g_k(z) = 1 + \frac{G_k(z - 1)}{1 - a_k(z - 1)}, \tag{4.35}$$

the output distribution is also geometric as in (4.31), with p.g.f.

$$H_N(z) = 1 + \frac{G_0(z - 1)}{1 - a(z - 1)}, \tag{4.36}$$

in which

$$G_0 = \prod_{k=1}^{N} G_k,$$

and a depends on the individual gains G_k and the coefficients a_k. The operations in (4.28) then constitute a sequence of homographic transformations of the complex plane that leave the point z = 1 invariant, and such transformations form a group. One might expect, therefore, that even if the single-stage distributions are not of the geometric type, the output distribution would approach the geometric form in (4.31) as the number of stages increases, the overall gain G_0 remaining fixed, and this behavior was demonstrated in [19]. Unlike the limiting behavior predicted by the central-limit theorem for sums, however, the variance of the output distribution of electrons continues to increase with an increasing number N of stages, even though its mean $G_0 = G^N$ remains fixed.

Although the limiting behavior of the output distribution as N increases has been extensively treated in the literature on branching processes, the emphasis

has been on the behavior of the random variable $W = G^{-N}n$ where n is the total number of output electrons, and the gain G per stage is kept fixed in the passage to the limit $N \to \infty$. The type of limiting behavior described in [19] seems not to have been considered.

References

[1] C. W. Helstrom, Trans. IEEE, AES-19, 428-437 (1983).

[2] S. O. Rice, Bell System Tech. J., 52, 707-722 (1973).

[3] C. W. Helstrom, Statistical Theory of Signal Detection, 2nd ed., Oxford: Pergamon Press (1968).

[4] C. W. Helstrom, Trans. IEEE, AES-14, 630-640 (1978).

[5] P. Swerling, Trans. IRE, IT-6, 269-308 (1960).

[6] J. V. diFranco, W. L. Rubin, Radar Detection, Englewood Cliffs, N.J.: Prentice-Hall (1968).

[7] C. W. Helstrom, J. C. Ritcey, "Evaluation of the noncentral F distribution by numerical contour integration", submitted to SIAM J. Sci. Stat. Comput.

[8] D. Slepian, Bell System Tech. J., 37, 163-184 (1958).

[9] C. W. Helstrom, "Calculation of cumulative distributions and detection probabilities in communications and optics," proposal submitted to AFOSR, 1982.

[10] T. Kailath, B.C. Levy, L. Ljung, M. Morf, Trans. IEEE, IT-24, 469-477 (1978).

[11] M. R. Hestenes, E. Stiefel, J. Res. NBS, 49, 409-436 (1952).

[12] T. Kailath, Trans. IEEE, IT-19, 750-760 (1973).

[13] C. W. Helstrom, SIAM J. Sci. Stat. Comput., 4, 353-356 (1983).

[14] C. W. Helstrom, S. O. Rice, "Computation of counting distributions arising from a single-stage multiplicative process," J. Comp. Phys. (to appear).

[15] G. Bédard, Phys. Rev., 151, 1038-1039 (1966).

[16] S. O. Rice, Bell System Tech. J., 47, 1971-2013 (1968).

[17] R. Lugannani, S. O. Rice, Adv. Appl. Prob., 12, 475-490 (1980).

[18] J. R. Prescott, Nucl. Instr. & Meth., 39, 173-179 (1966).

[19] C. W. Helstrom, "Output distributions of electrons in a photomultiplier," submitted to J. Appl. Phys.

Papers prepared under Grant AFOSR-82-0343

C. W. Helstrom, S.O. Rice, "Computation of counting distributions arising from a single-stage multiplicative process," to appear in Journal of Computational Physics.

C. W. Helstrom, J. C. Ritcey, "Evaluation of the noncentral F-distribution by numerical contour integration," submitted to SIAM Journal of Scientific and Statistical Computation.

C. W. Helstrom, "Output distributions of electrons in a photomultiplier," submitted to Journal of Applied Physics.

Persons employed on Grant AFOSR-82-0343

Carl W. Helstrom, principal investigator

Stephen O. Rice, consultant (unsalaried)

James C. Ritcey, graduate research assistant

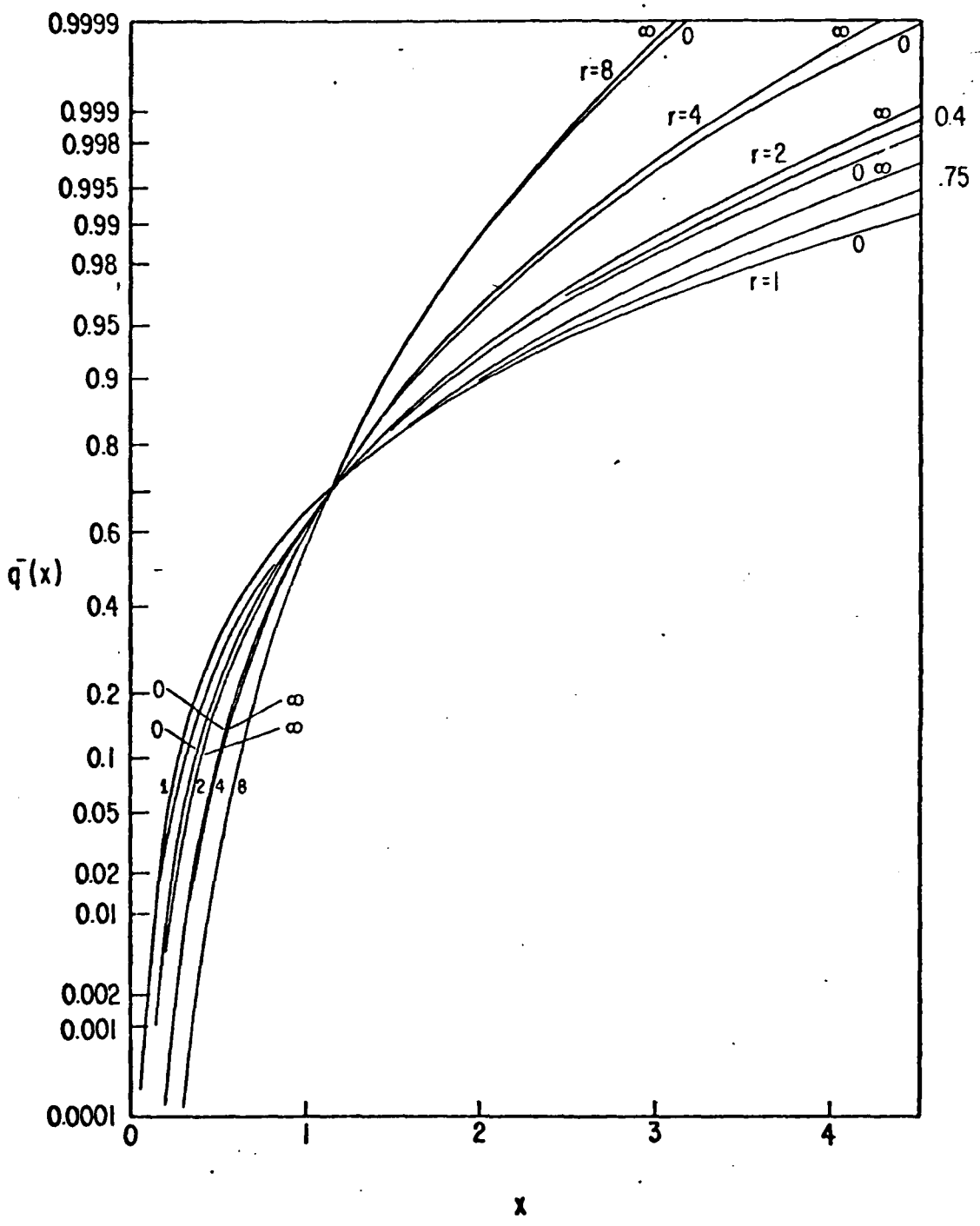

Fig. 1. Cumulative distribution $\bar{q}(x)$ of average power of RLC noise. Intermediate curves are indexed on the right with the value of Q.

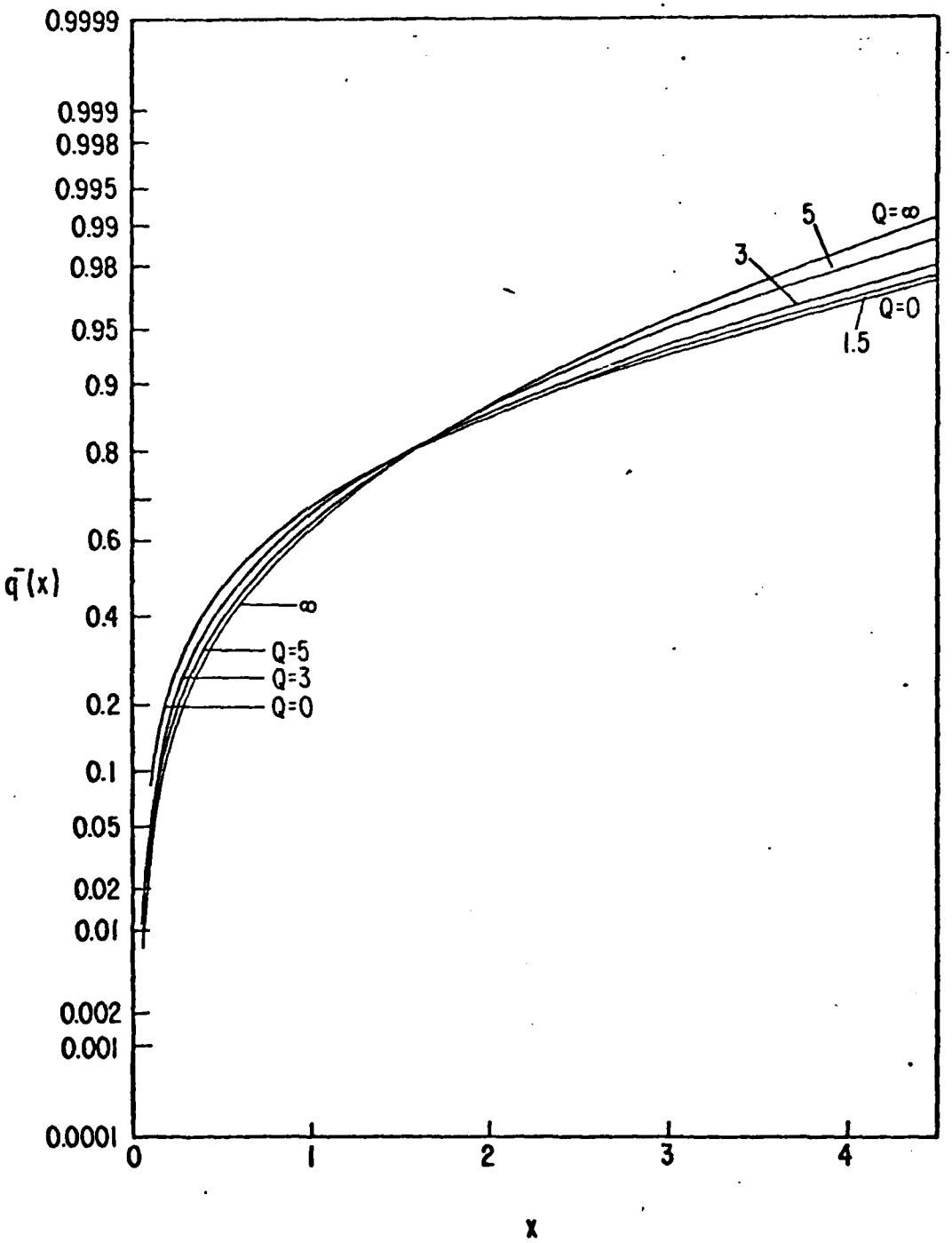

Fig. 2. Cumulative distribution $\bar{q}(x)$ of average power of RLC noise: r = 0.2. Curves are indexed with the value of Q.

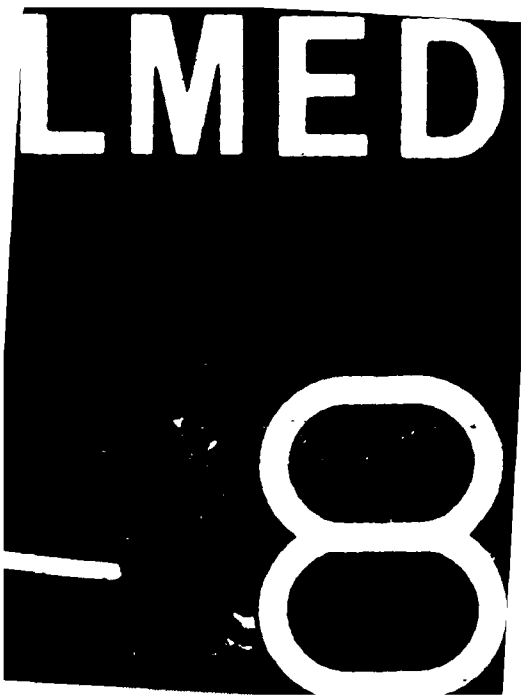
LMED
8